Journal of Structural Geology, Vol. 11, No. 3, pp. 231 to 244, 1989
Printed in Great Britain

0191-8141/89 $03.00 + 0.00

Asymmetric quartz *c*-axis fabrics and flow vorticity: a study using rotated garnets

R. L. M. VISSERS

Department of Structural and Applied Geology, Institute of Earth Sciences, Budapestlaan 4, 3508 TA Utrecht, The Netherlands

(*Received* 9 *June* 1987; *accepted in revised form* 9 *August* 1988)

Abstract—The development of a type I crossed-girdle *c*-axis fabric with an asymmetric density distribution and an internally asymmetrical skeletal outline is examined in a specimen of garnet bearing mylonitic quartzite from the Betic Movement Zone in southern Spain. The garnets are pre-mylonitic skeletal porphyroblasts that rotated during mylonitic deformation but preserved a strain-free equilibrium microstructure and a random *c*-axis fabric. It follows that the asymmetry of the density distribution must result from the deformation history itself. The sense of asymmetry of the *c*-axis population and that of the skeletal outline are consistent with the sense of vorticity inferred from extensional crenulations and asymmetric microboudinage, and also with the sense of rotation of the garnets. Analysis of the rotation angles with aspect ratio of the garnet porphyroblasts demonstrates that a pure shear component was involved in an essentially non-coaxial flow. This may explain the internal asymmetry of the fabric skeleton, and confirms the idea that a spectrum exists of type I fabrics intermediate between the theoretically predicted fabrics for pure and simple shear. A tentative reconstruction of the kinematic framework suggests that the central segment of the fabric skeleton is linked to the extensional apophysis of the flow.

INTRODUCTION

VARIOUS studies of quartz *c*-axis preferred orientation patterns have focused on their potential use as indicators of the sense of vorticity in non-coaxial deformation histories. These studies include theoretical predictions (Etchecopar 1974, 1977, Lister *et al.* 1978, Lister & Hobbs 1980) as well as analyses of natural quartz *c*-axis fabrics developed in non-coaxial crystal–plastic flow. In studies concerned with natural *c*-axis patterns, asymmetric fabrics are commonly interpreted in the light of a sense of shear inferred from shear zone geometries (Carreras *et al.* 1977, Roermund *et al.* 1979, Simpson 1980, Garcia Celma 1983), regional evidence for large-scale movements of adjacent rocks (Bouchez & Pêcher 1981, Behrmann & Platt 1982, Law *et al.* 1984) or independent microstructural evidence (Eisbacher 1970, Simpson & Schmid 1983, Lister & Snoke 1984, Mancktelow 1987). Such studies give increasing confidence that asymmetric fabrics have a systematic relationship with the sense of non-coaxiality (see e.g. Schmid & Casey 1986). However, a number of workers emphasize that asymmetric fabrics may be unreliable in this respect (Lister & Williams 1979, Passchier 1983, Simpson & Schmid 1983) and that they are kinematic indicators which must be used with care, in particular when other criteria for the sense of vorticity are lacking.

One problem in many quartz fabric studies is the scarcity of data on the *c*-axis orientation distribution prior to fabric development. An initially non-random distribution of *c* axes may result in asymmetrically populated fabric skeletons Lister & Williams 1979) and this complicates the use of asymmetric fabrics to infer the sense of vorticity in non-coaxial flow. Another problem met in the study of natural *c*-axis fabrics is the lack of independent constraints on the flow regime and deformation history which controlled the development of the fabric within a given volume of deformed rock. These problems are in part overcome in fabric studies of heterogeneous simple shear zones (Carreras *et al.* 1977, Roermund *et al.* 1979, Garcia Celma 1983). Quartz *c*-axis patterns sampled near a shear zone boundary or outside a shear zone are likely to reflect the pre-deformation orientation distribution of *c*-axes from which the fabric in the shear zone developed while for example, in the case of clearly undeformed wallrocks, some constraints may be placed on the flow regime.

This study discusses the development of an asymmetric quartz *c*-axis pattern in a garnet–chloritoid–mica quartzite from a greenschist-facies movement zone in the Betic Zone of southern Spain (Fig. 1). The garnets in this rock developed as non-spherical skeletal porphyroblasts along the grain boundaries of a foliated quartzite matrix and included large numbers of quartz grains during growth, thus preserving the microstructure and a random *c*-axis distribution as armoured relic fabrics. The internal planar fabrics in the garnets make variable angles to the external foliation in the rock indicating a post-garnet phase of ductile deformation. This deformation led to the development of an asymmetric *c*-axis fabric in the quartzite matrix, in a flow regime which can be estimated from a quantitative analysis of the porphyroblast rotation angles as a function of their aspect ratio.

GEOLOGICAL SETTING OF THE SPECIMEN

The Alpine Betic Zone in southern Spain is made up of two groups of nappe units (Torres Roldan 1979). The lowest group, referred to as the Nevado-Filabride complex (Egeler & Simon 1969), consists of upper green-

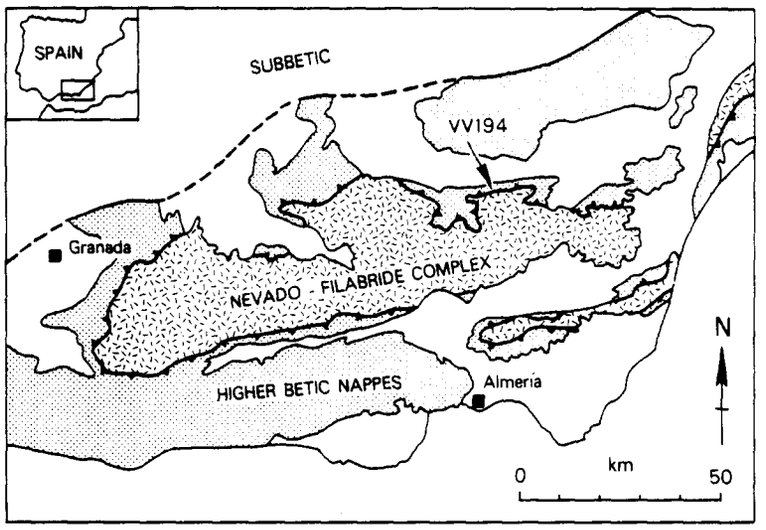

Fig. 1. Tectonic sketch map of the central and eastern Betic Zone showing location of specimen VV 194 in the contact zone (Betic Movement Zone, heavy line with teeth) between the Nevado-Filabride complex and higher Betic units. Tectonic contact between Betic Zone and undifferentiated Subbetic rocks to the N indicated by heavy line. Unornamented areas in Betic Zone are Neogene and Quaternary deposits.

schist to amphibolite-facies rocks of sedimentary and igneous origin, which contain relics of an early Alpine high pressure, low temperature metamorphism (de Roever & Nijhuis 1963, Puga 1971, Vissers 1977, 1981, Diaz de Federico *et al.* 1978). These rocks are overlain by the allochthonous higher Betic units of low and locally medium metamorphic grade. Relics of a metamorphic zoning in these units reflect an early pre-nappe metamorphism characterized by medium to low pressure, high temperature facies series (Westra 1969, Torres Roldan 1979). The contact between the two groups of units is marked by a zone of intense, mostly ductile deformation related to nappe emplacement, referred to as the Betic Movement Zone by Platt & Vissers (1980), and characterized by the development of mylonites (Behrmann & Platt 1982, Platt 1982, Platt *et al.* 1984, Platt & Behrmann 1986) and/or a zone of calcareous cataclasites (Leine 1968, Vissers 1981).

The specimen (VV 194) was taken from a 30 m thick block of mylonitic garnet–chloritoid–mica quartzite embedded in calcareous cataclasites underneath the higher Betic units in the northern Sierra de los Filabres (Fig. 1). The occurrence of this and similar mylonitic quartzite and micaschist blocks in calcareous cataclasites presumably indicates relatively late movements along the main thrust contact at shallow crustal levels. Unfortunately, this tectonic setting precludes any conclusion of local geological interest with regard to the direction of nappe emplacement, as unknown rigid-body rotations of the blocks during cataclasis will have disturbed possible pre-existing relationships between the sense of shear during crystal–plastic flow and the geometry of the overriding nappe.

GEOMETRY AND MICROSTRUCTURE OF THE SPECIMEN

Specimen VV 194 is an S tectonite, with a distinctly platy foliation parallel to a compositional layering (Fig. 2). This foliation is defined by the parallel arrangement of flakes of colourless mica (Figs. 3a & b) up to 0.5 mm

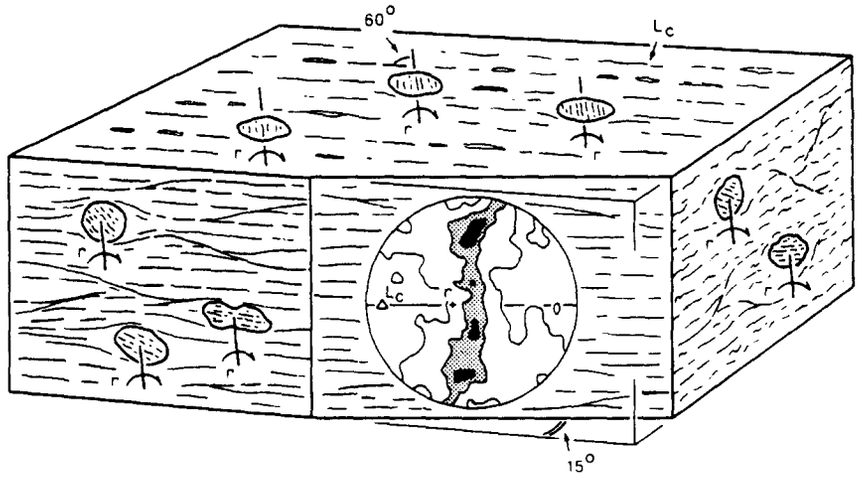

Fig. 2. Block diagram showing geometry of the sample and orientation of the *c*-axis fabric with respect to the porphyroblast rotation axes (*r*). L_r is the crenulation lineation. Note that the fabric is shown in a plane at approximately 15° to the weak crenulations.

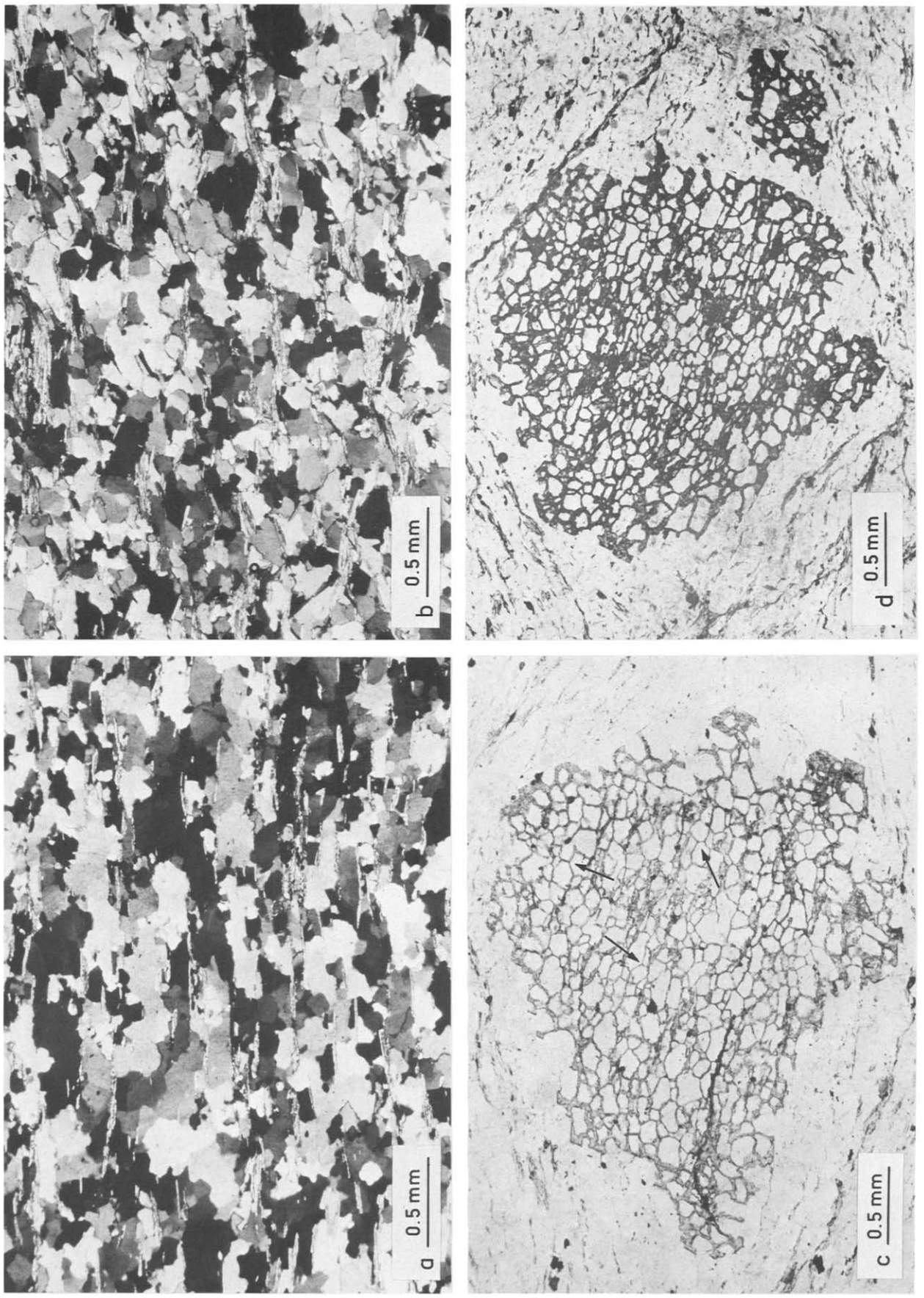

Fig. 3. (a) Microstructure of the mica quartzite in section parallel to crenulations, crossed nicols at 45° to foliation. (b) Same as (a) but section perpendicular to crenulations, crossed nicols at 45° to foliation. (c) Garnet porphyroblast with included quartz microstructure, section parallel to crenulations; plane polarized light. Note various relic triple point contacts (arrows). (d) Garnet porphyroblast with numerous quartz inclusions delineating an internal fabric, section perpendicular to crenulations; plane polarized light.

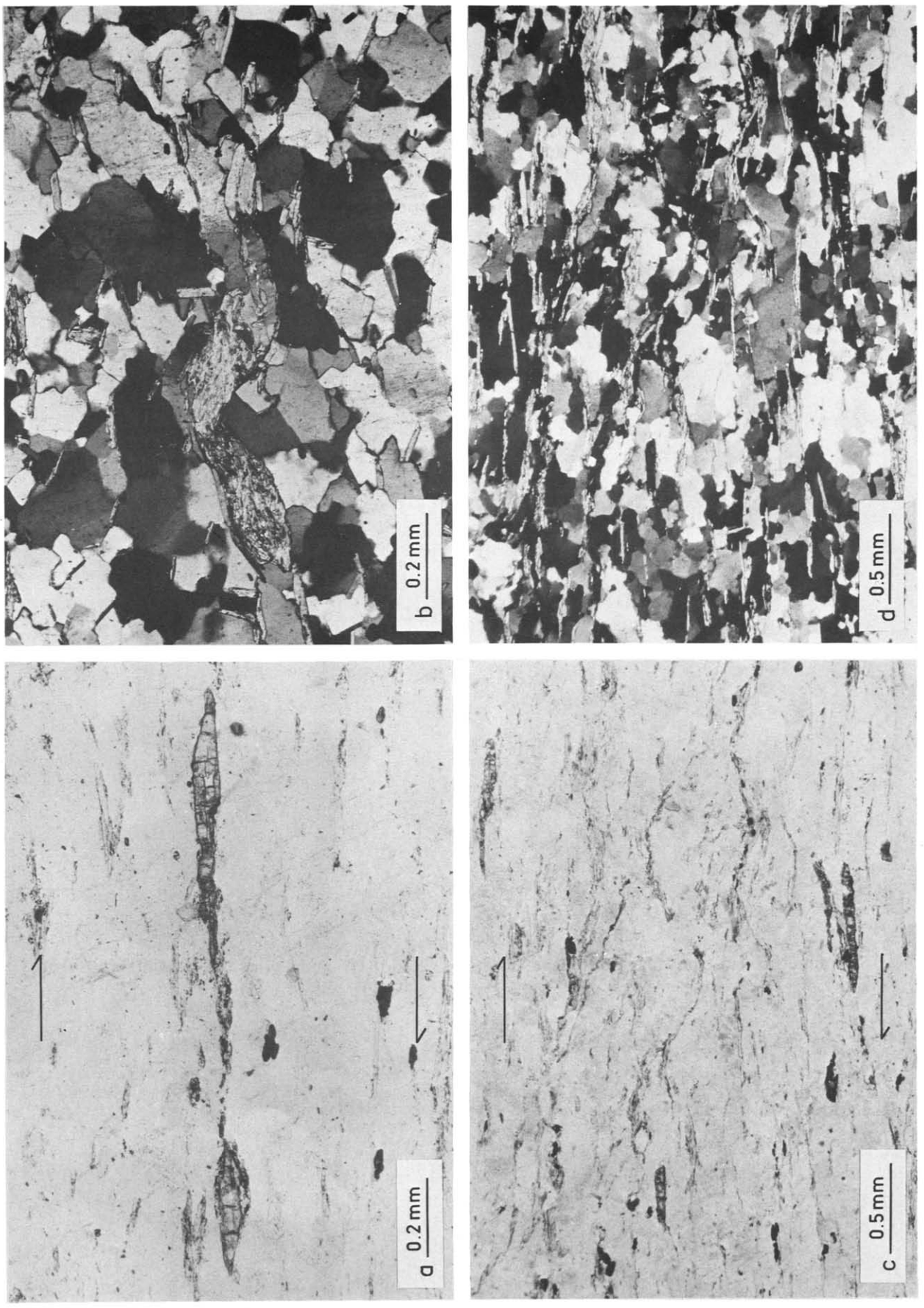

Fig. 4. Microstructures indicating extension of the foliation. (a) Asymmetric microboudinage of chloritoid suggesting dextral shear component, section parallel to crenulations; plane polarized light. (b) Crenulated microboudin of colourless mica, section perpendicular to crenulations, crossed nicols at 45° to foliation. (c) Extensional crenulations of the foliation, same section as in (a); plane polarized light. Note predominance of right-dipping set suggesting dextral shear. (d) Same as (c) crossed nicols at 45° to foliation.

long, and more or less evenly distributed in a quartzite matrix. Inequant grains of the quartz and oriented crystals of chloritoid, about 0.5 mm across, contribute to the foliation microstructure. The foliation bends around large porphyroblasts of garnet, up to 4 mm in diameter, which show straight inclusion patterns described below, mostly at low to moderate angles of up to 50° with the foliation in the matrix (Figs. 2 and 3c & d). The foliation is deformed by high and low angle conjugate sets of extensional crenulation cleavages (Platt & Vissers 1980), but there is no clear extension lineation developed. In addition, the foliation is affected by a set of weak crenulations which cause a faint lineation in the foliation plane.

Microstructures within the matrix

The quartz grains in the matrix show a bimodal grain size distribution with large (up to 400 μm) and small (50–100 μm) grains defining a coarsely sutured microstructure (Figs. 3a & b). The large grains show intracrystalline deformation features such as subgrains at 50 μm scale, deformation bands and occasional deformation lamellae. They have inequant shapes in sections parallel to the weak crenulation lineation, and in these sections they are bounded by micas with a strong preferred orientation (Fig. 3a). In sections perpendicular to this lineation with a more variable orientation of the mica grains, the long dimensions of the quartz grains are less pronounced (Fig. 3b). The small quartz grains, however, with dimensions less than the distance between nearby mica crystals, are about equidimensional in both sections. In addition, quartz–quartz interfaces are commonly perpendicular to the (001) boundaries of adjacent mica grains, or are pinned at the ends of mica crystals. These observations strongly suggest control exerted by the micas on the grain shapes of the quartz during grain boundary migration.

The mica and chloritoid crystals have pinched ends and are microboudinaged, indicating a component of extension along the foliation. One example was observed of asymmetric fish-type microboudinage of chloritoid suggesting a shear component (dextral in Fig. 4a) consistent with the extensional crenulation cleavages which show a tendency for a dextral set of these cleavages to dominate (Figs. 2 and 4c & d). The extensional cleavages and the microboudins of mica are affected by the weak crenulations (Fig. 4b) indicating that the deformation which produced the extensional structures predates the shortening associated with these crenulations.

Microstructures within the garnets

The garnet porphyroblasts include many quartz grains (Figs. 3c & d), and are in fact made up of quartz inclusions bound together by a skeleton of garnet grown in the quartz–quartz interfaces as well as at the expense of local mica and chloritoid grains. The quartz grains define an internal fabric in the porphyroblasts (Figs. 3c & d), are equant to slightly inequant and have grain sizes of 100–200 μm. They are strain free, and adjacent quartz grains show triple point contacts now occupied by a thin film of garnet (Fig. 3c). The internal fabric in the garnets makes a moderate angle with the external foliation in the matrix and can commonly be traced into this foliation, indicating prekinematic growth (Zwart 1962). The external foliation bends around the porphyroblasts such that symmetric to slightly asymmetric deformation shadows are developed adjacent to the garnets, a phenomenon consistent with a component of flattening normal to the foliation.

The garnets show partial replacement by fine-grained chlorite. As chlorite is probably incapable of maintaining the shape of the garnets during significant deformation of the matrix, this alteration is ascribed to a stage of postkinematic retrogression, known from many of the adjacent rocks in the Betic Zone (Puga 1971, Vissers 1981).

The above observations suggest growth of the garnets under essentially static conditions in a foliated quartzite with a strain-free equilibrium microstructure and grain size of 100–200 μm. This blastesis occurred prior to a deformation which caused rotation of the garnets and extension of the foliation and induced a grain size reduction of the quartz down to at least 50 μm scale as well as grain growth, presumably as the result of both rotation and migration recrystallization (Poirier & Guillopé 1979). The development of the microstructure was probably dominated by migration recrystallization during the later stages of this deformation and during subsequent crenulation of the foliation. The metamorphic conditions during deformation and garnet rotation can at best be estimated at mid to low greenschist facies.

QUARTZ *c*-AXIS PATTERNS

Quartz *c*-axis fabrics have been measured in the matrix and within two garnet porphyroblasts (shown in Figs. 3c & d). To avoid effects of local heterogeneities, the *c* axes in the matrix were measured in a domain (Fig. 3a) away from porphyroblast deformation shadows and extensional crenulations. Two thin sections perpendicular to the foliation were used to measure the fabrics, one parallel to the weak crenulation lineation and one perpendicular to this lineation. The fabrics have been rotated about the normal to the foliation in order to represent them all in the same viewing direction, with one of the estimated symmetry axes of the fabric in the matrix perpendicular to the plane of the paper. The orientation of this fabric with respect to the geometry of the specimen is shown in Fig. 2.

There is a significant difference between the quartz fabrics in the porphyroblasts and the fabric in the matrix. The *c* axes in the porphyroblasts do not show clear patterns or obvious pole-free areas, and the fabrics appear random (Figs. 5a & b). The *c* axes in the matrix

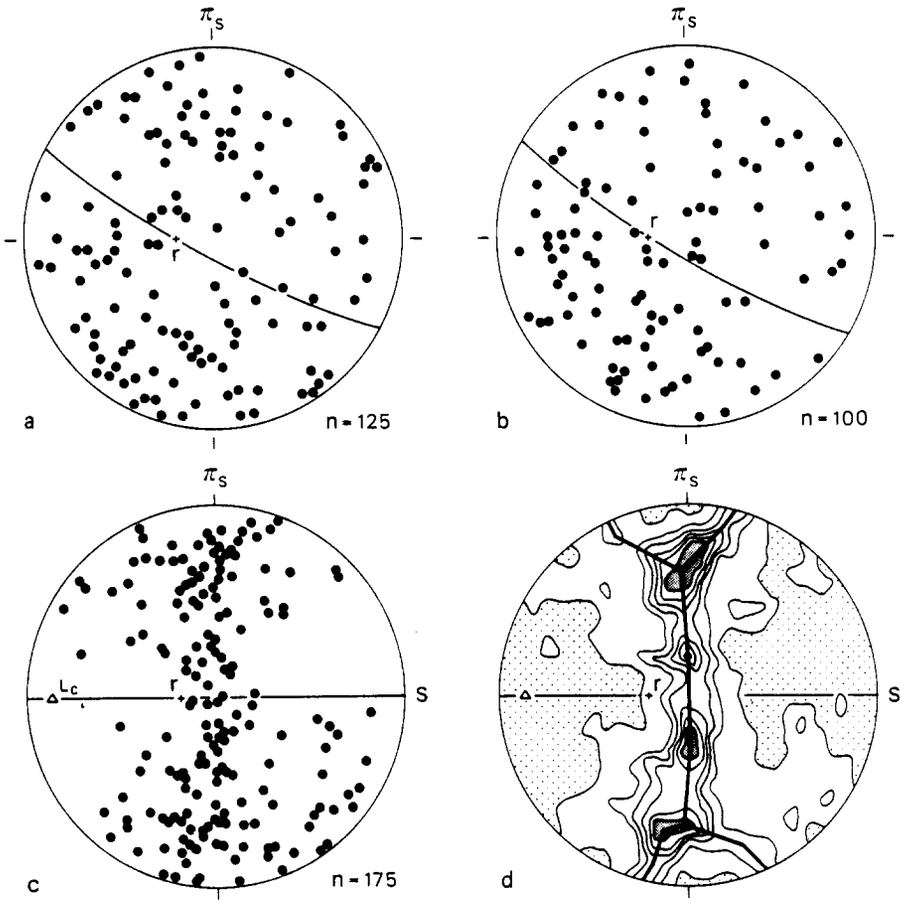

Fig. 5. Quartz *c*-axis fabrics in sample VV 194. All pole figures are equal-area, lower-hemisphere projections, represented with the same orientation as shown in Fig. 2. *S* denotes foliation, π_s the pole to the foliation, *r* the mean rotation axis of the garnets and L_c the crenulation lineation. (a) Quartz *c*-axes in the garnet porphyroblast shown in Fig. 3(c). (b) Quartz *c*-axes in the porphyroblast shown in Fig. 3(d). (c) Quartz *c*-axes in the matrix of the sample, in the domain shown in Fig. 3(a). (d) Contoured pattern of the *c*-axes measured in the matrix in (c), contours at 0.6, 1.7, 2.3, 2.9, 4.0 and 4.6% (shaded) in 1% area, with fabric skeleton and accentuated pole-free areas (light stipple).

(Fig. 5c) show an asymmetric intensity distribution with distinct maxima, disposed along the skeletal outline (Lister & Williams 1979) of a type I crossed girdle (Lister 1977) which itself shows a slight internal asymmetry due to an unequal inclination of the peripheral legs with respect to the central girdle segment (Fig. 5d). Note that this central segment of the fabric skeleton is perpendicular to the foliation, but that the pole free areas lie decidedly oblique to the foliation and the central segment of the fabric.

The above observations suggest that the *c*-axis fabric in the matrix developed during the deformation which led to rotation of the garnets, changes of the quartz microstructure and extension of the foliation. Comparison of the fabric with theoretically predicted quartz *c*-axis patterns (Lister 1977, Lister & Hobbs 1980) and with *c*-axis fabrics reported from studies of naturally deformed quartzites (Behrmann & Platt 1982, Law *et al.* 1984, Schmid & Casey 1986, Mancktelow 1987) suggests a plane strain deformation history with a dextral sense of vorticity and, possibly, a shear direction in the plane of the foliation. However, theoretical studies of quartz fabric development (Lister 1974, Lister *et al.* 1978, Lister & Hobbs 1980) have emphasized that the characteristics of the *c*-axis patterns are controlled by the orientation of the kinematic framework and the deformation path, and that for a given deformation history the intensity of the fabric increases with increasing strain. It is therefore desirable to put as many constraints as possible on the kinematics of the deformation and on the magnitude and orientation of the strain accumulated during fabric development. The following analysis serves to obtain such information from the rotated garnet porphyroblasts.

ANALYSIS OF GARNET PORPHYROBLAST ROTATION

Various workers have studied the relationship between the amount of porphyroblast rotation and the magnitude of the associated strain (Schmidt 1918, Ramsay 1962, Rosenfeld 1970, Ghosh & Ramberg 1976, Schoneveld 1979) and both simple shear, pure shear and a combination of these have been shown to be capable of producing such rotations. In the case of spherical porphyroblasts application of such analyses is necessarily difficult in view of the common lack of constraints on the deformation history. For moderate to low rotation angles in particular, simple shear and pure shear

histories may yield completely equivalent rotations (see e.g. Powell & Treagus 1970). However, within the limits of a number of assumptions, the amounts of rotation of non-spherical porphyroblasts with a range of aspect ratios may yield information on the flow regime and on the magnitude and orientation of the strain. In order to obtain this information from the rotated garnets we will interpret the rotation data with reference to existing theory on reorientation of ellipsoidal bodies, embedded in a viscous medium subjected to simultaneous pure and simple shear flow.

Observations

Irrespective of thin section orientation, many garnets in the specimen studied show inequant shapes, with the internal fabric parallel to the long dimensional axes. The mean aspect ratio of the garnets is about the same for sections parallel and perpendicular to the lineation (1.33 and 1.30, respectively) suggesting that these garnets approximate an axially symmetric, oblate spheroidal shape, with two long dimensional axes in the plane of the internal foliation (Fig. 2). In addition, strongly inequant shapes are clearly due to coalescence of two or even three garnets, and all porphyroblasts with an aspect ratio larger than 2 belong to this category. Such coalesced porphyroblasts were only observed in sections parallel to the lineation.

For a quantitative study of the observed rotations it is essential to know the orientations of the rotation axis. One obvious reason is that cut effects in oblique sections induce a reduction of the rotation angles. However, more important may be the fact that the rotation axis is not physically stored in postcrystalline rotated porphyroblasts as it is in synkinematic rotational inclusion patterns, and that a problem arises when the true rotation axis does not lie in the foliation plane throughout the deformation (Vissers 1987). Such a situation may occur when the foliation behaves as a mechanically passive marker, an assumption often made in theoretical studies of porphyroblast rotation. The apparent rotation axis, defined by the intersection of the internal and external fabric, does not necessarily coincide in such cases with the true axis of rotation, and apparent rotation angles between internal and external fabric may yield underestimated values of the associated strains (Vissers 1987).

Differently oriented saw cuts perpendicular to the foliation were used to cut a number of garnets in two directions in order to determine directly the orientation of the internal fabric and its intersection with the external foliation. The apparent rotation axes thus measured show a remarkable consistency within some 10° which indicates that, given the variable rotation angles, these intersections represent true rotation axes (Vissers 1987). A thin section parallel to the foliation confirmed this result. The orientation of the mean rotation axis (r) determined from the direct measurements is shown in Fig. 2 and in the pole figures of Fig. 5, and it lies approximately 15° away from the intersection of the crossed-girdle fabric skeleton and the foliation.

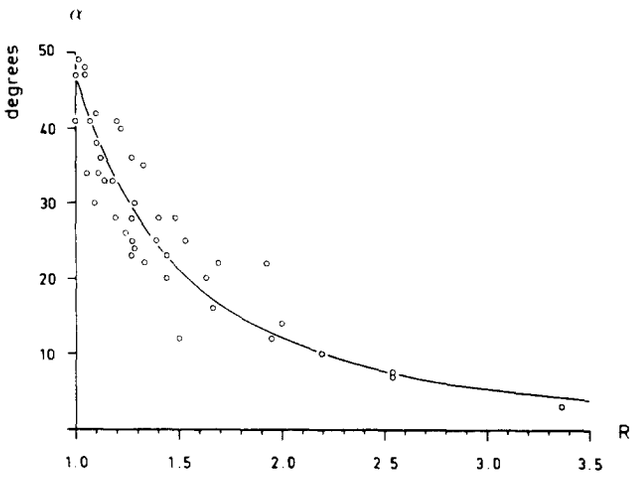

Fig. 6. Diagram showing rotation angle α vs aspect ratio R of 43 garnet porphyroblasts measured, in sections perpendicular to the mean garnet rotation axis, as the angle between the linear inclusion trails and the foliation in the matrix. The best-fit curve, calculated as the linear regression curve of log–log transformed measurements, yields a rotation angle of 47.1° for spherical porphyroblasts.

Sections perpendicular to the mean rotation axis were used to measure 43 garnet aspect ratios and rotation angles. All porphyroblasts in these sections show the same sense of dextral rotation, which coincides with the sense of shear inferred from the extensional cleavages, asymmetric microboudinage and quartz fabric asymmetry. The results of the measurements are shown in Fig. 6. It emerges that the rotation angle (α) varies such that the largest angles occur in equant garnets and that these angles decrease with increasing aspect ratio (R). A best-fit curve has been calculated as a linear regression curve of log–log transformed measurements and has a correlation coefficient of -0.94. The intercept value yields a rotation angle with respect to the foliation of 47.1° for spherical porphyroblasts.

Analysis of the rotation data

The quantitative account of the reorientation of inclusions in a viscous medium by Ghosh & Ramberg (1976) seems particularly applicable to the data presented here. On the basis of their equations for the finite rotation of an ellipsoidal object, porphyroblast rotation angles α have been calculated as a function of aspect ratio R for a range of values of ϕ_0 and s_r, ϕ_0 being the initial orientation of a porphyroblast, equal in this case to the initial orientation of the foliation (see Appendix), and s_r the ratio of the rates of pure to simple shear, defined as shown in Fig. 7 (see Appendix for further details). The procedure involved determination by trial and error of the shear strain γ at chosen values of ϕ_0 and s_r, so as to obtain the best fit intercept value of 47.1° for a spherical porphyroblast, followed by calculation of the $R - \alpha$ curve for those values of γ,ϕ_0 and s_r. It emerges that a good fit of theoretical α values and the observed rotation

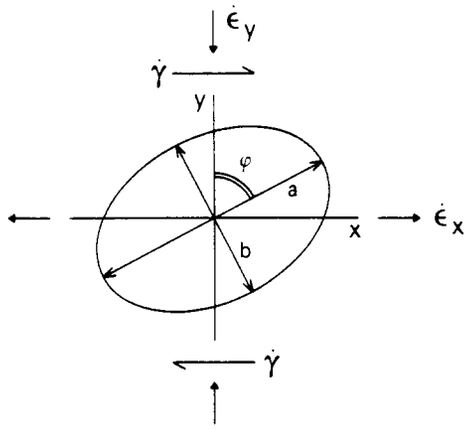

Fig. 7. Diagram showing the geometrical relationship between components of pure and simple shear in Ghosh & Ramberg's (1976) analysis, x and y axes are parallel to the directions of the principal strain rates $\dot{e}_x$ and $\dot{e}_y$ of the pure shear component, x is parallel to the shear direction of the simple shear component $\dot{\gamma}$. Note that the orientation φ of an ellipsoidal object with long and short dimensional axes a and b is measured with respect to the normal to the shear direction.

angles is possible for a variety of initial orientations, but only for a limited range of s_r values of about 0.5–0.7. This is illustrated in Fig. 8(a) which shows curves for a range of initial orientations, and in Figs. 8(c) & (d) in which the best-fit curve is bracketed between the curves for s_r values of 0.5 and 1.0. The s_r value may be somewhat higher (between 0.9 and 1.1) at initial orientations of the order of 120°. Moreover, it was found impossible to obtain a good fit with the data for $s_r = 0$, that is to say for purely simple shear (Fig. 8b), irrespective of the initial orientation of the foliation and the porphyroblasts. At values of s_r of the order of 1 and larger the curves also deviate considerably from the best fit curve. The effect of s_r, hence of the flow regime, on the $R - \alpha$ curves is illustrated in Figs. 8(c) & (d).

Assumptions and limitations of the analysis

An accurate description of the flow regime on the basis of a Ghosh & Ramberg (1976) approach of porphyroblast rotation data relies heavily on the following assumptions underlying their analysis.

(1) The porphyroblasts behave as rigid objects in a viscous matrix.

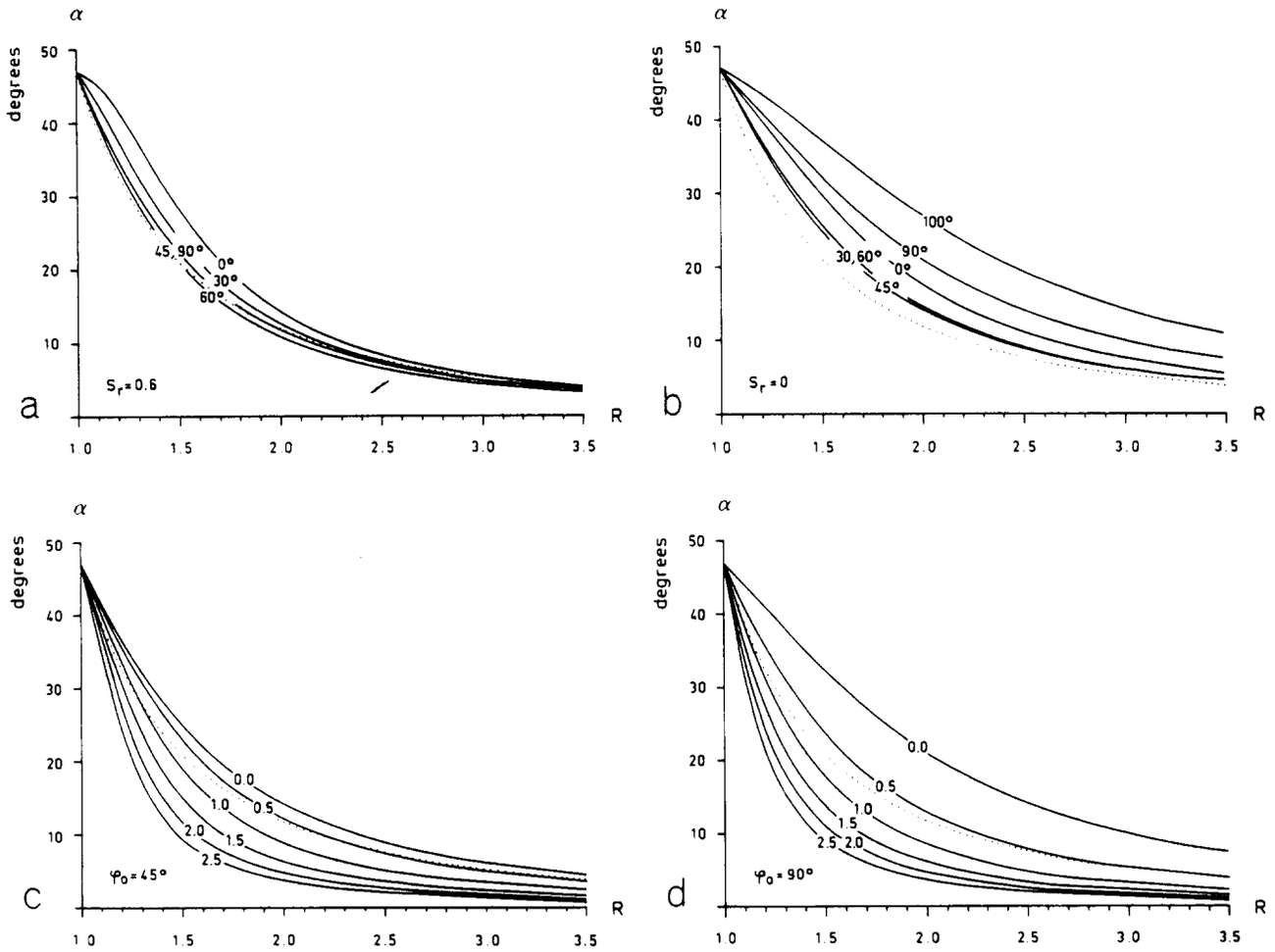

Fig. 8. Calculated $R - \alpha$ graphs for a number of initial orientations of the porphyroblasts and foliation and for various values of s_r. The best-fit curve to the data (dotted) is shown for reference. (a) For the various initial orientations shown and $s_r = 0.6$. (b) For the initial orientations shown, but $s_r = 0$, hence strictly simple shear. (c) For the initial orientation $\varphi_o = 45°$ and, from upper to lower curve, for increasing values of s_r between 0 and 2.5. (d) Same as (c) but initial orientation $\varphi_o = 90°$ (shear component with shear direction parallel to the foliation). For further discussion see text.

(2) One symmetry axis of the porphyroblast-like objects is parallel to the rotation axis, and perpendicular to the plane of the essentially two-dimensional analysis.

(3) The flow regime is either simple shear or plane strain flow with simultaneously operating pure and simple shear components.

(4) Foliations behave as mechanically passive marker planes.

The lack of deformational features in the skeletal garnets and included quartz grains suggests that the garnets behaved as rigid objects during rotation, and that this assumption does not impose any particular problem.

As to the second assumption it can be noted that the nearly oblate spheroidal shape of the garnets with two long dimensional axes in the plane of the internal foliation implies that sections perpendicular to the rotation axis will contain the short dimensional axis and a long dimension. This means that the symmetry requirement following from the second assumption is fulfilled for these sections. There is an angle of 15°, however, between the mean garnet rotation axis and the fabric intersection with the foliation, while they should ideally coincide. This may indicate that the rotation axis did not remain perfectly normal to the plane of the analysis.

The restriction to a plane strain history may pose a problem. The type I crossed-girdle fabric suggests plane deformation in the specimen. However, the 15° angle between the mean rotation axis and the fabric symmetry axis could also be related to a deviation from plane strain flow. The setting of the specimen in the Betic Movement Zone, which given its tectonic position was undoubtedly a zone of shear (Platt *et al.* 1984, Platt & Behrmann 1986), equally suggests that the assumption of a plane strain history is reasonable, but does not exclude deviations from plane deformation. There are no strain markers available to put independent constraints on the deformation history, and the assumption of plane deformation in the specimen remains unsubstantiated.

The fourth assumption underlying Ghosh & Ramberg's (1976) analysis concerns a mechanically passive behaviour of the foliation during flow. However, the extensional structures affecting the foliation indicate a mechanically active behaviour of the foliation. Platt (1984) has suggested that, irrespective of the nature of the bulk flow, a likely way of accommodating such a mechanical anisotropy within a given domain is that, at the scale of the domain, the flow becomes partitioned into slip along the foliation, stretch of the foliation, and spin of the entire domain. It is emphasized here that the spin component is undetectable within the domain itself where the shear component becomes attached to an extending foliation. This implies a local kinematic framework at the scale of the domain controlling the development of the fabrics and microstructures (see also Lister & Williams 1979). With these considerations in mind the analysis may be simplified to the case of an initial orientation of the foliation and the porphyroblasts parallel to the local shear direction. This allows a more accurate determination of s_r with a predicted $R - \alpha$ curve fitting optimally with the garnet rotation data. A value of $s_r = 0.65$ is obtained, and the resulting graph is shown in Fig. 9.

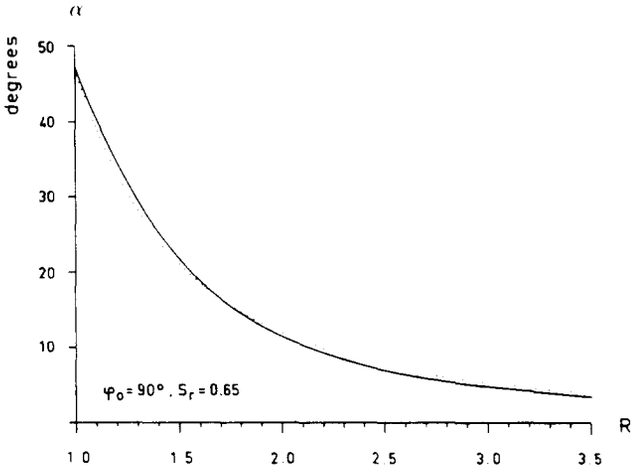

Fig. 9. Calculated $R - \alpha$ curve for initial orientation $\varphi_0 = 90°$ and $s_r = 0.65$, showing optimal coincidence with best-fit curve to the data (dotted).

Alternative deformation histories

Implicit in Ghosh & Ramberg's (1976) analysis is a flow regime characterized by *simultaneous* pure and simple shear components, hence a deformation history with a time–constant flow ratio of these components and a constant kinematic framework. Alternative deformation histories can be envisaged involving changes of the s_r value with time. Two cases have been explored as an example. Figure 10(a) shows an $R - \alpha$ curve which fits reasonably well the observed rotation data and results from initial simple shear flow ($s_r = 0$), followed by a pure shear overprint (with $e_x = 0.55$). Likewise, a deformation history involving initial deformation in a flow regime with $s_r = 0.2$ followed by a pure shear overprint with $e_x = 0.35$ can explain the observed garnet rotations (Fig. 10b). In each case the non-coaxial component of the flow during the first stage produces the entire finite rotation of the spherical porphyroblasts, while non-spherical ones rotate further during the coaxial pure shear overprint. The finite strains built up in these alternative histories differ but, because independent strain markers in the specimen are lacking, this criterion cannot be used here to distinguish between such histories. They are possible alternatives which can only be evaluated in relation to the development of the quartz fabric. This point is further discussed below.

DISCUSSION

c-axis fabric and kinematic framework

The above analysis indicates that the *c*-axis fabrics of Figs. 5(c) & (d) developed in a non-coaxial deformation history with a pure shear component, either simultaneous with a component of simple shear or as a later

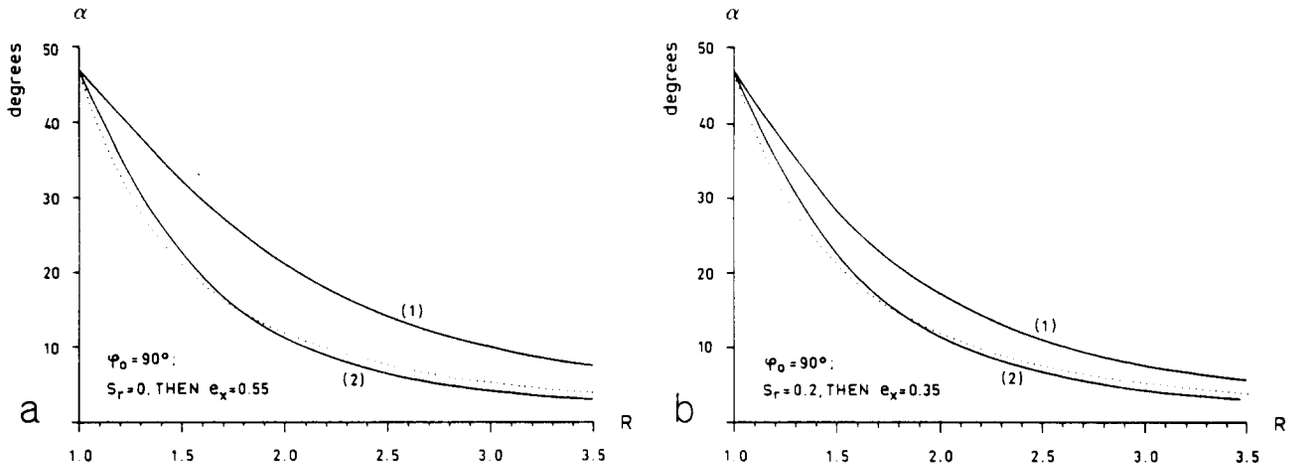

Fig. 10. Calculated $R - \alpha$ curves for two-stage deformation histories, initial orientation $\varphi_0 = 90°$. (a) Simple shear history ($s_r = 0$, upper curve, 1), followed by pure shear overprint with $e_x = 0.55$ (lower curve, 2). (b) Non-coaxial deformation history ($s_r = 0.2$, upper curve, 1) followed by pure shear overprint with $s_x = 0.35$ (lower curve, 2). Note that both two-stage histories (a and b) result in a reasonable coincidence with the best-fit curve (dotted).

overprint. Quartz *c*-axis fabrics with similar internal asymmetry have been described elsewhere (Behrmann & Platt 1982, Law *et al.* 1984, Platt & Behrmann 1986), and attributed to flow regimes deviating from simple shear. Similarly, Schmid & Casey (1986) have suggested flow regimes intermediate between pure and simple shear to explain a spectrum of internally asymmetric *c*-axis fabrics.

Platt & Behrmann (1986) have emphasized that the Taylor–Bishop–Hill simulations by Lister & Hobbs (1980) demonstrate the development of a central girdle segment, orthogonal to the shear plane in progressive simple shear and orthogonal to the XY plane in progressive pure shear. They stress that the shear plane in simple shear is a plane of zero angular velocity and that the X and Y directions in pure shear are lines of zero angular velocity with respect to the instantaneous stretching axes. For any non-coaxial plane strain flow intermediate between pure and simple shear two planes exist which intersect along the vorticity vector and in which lines perpendicular to the vorticity vector have zero angular velocity. These planes have been termed flow apophyses by Ramberg (1975) and represent eigenvector planes of the velocity gradients tensor (Passchier 1986). In a Mohr circle for flow (Lister & Williams 1983, Means 1983, Passchier 1986, 1987a) the orientations of the apophyses follow from the intersections with the stretching rate axis (Fig. 11a), which implies that the angle between the extensional and shortening apophyses depends on the degree of non-coaxiality only (Passchier 1986). They are perpendicular in pure shear and coincide in the flow plane in simple shear.

Passchier (1987a) has shown that the x direction in Ghosh & Ramberg's (1976) analysis (the shear direction of the simple shear component, Fig. 7) coincides with the extensional flow apophysis. It was argued above that the mechanical anisotropy due to the foliation would induce partitioning of a bulk flow into shear along the foliation, stretch of the foliation, and spin of the system. It follows that, given such a partitioning, the extensional apophysis of the local flow becomes attached to the foliation. In addition, we have already noted that the central girdle segment of the *c*-axis fabric is perpendicular to the foliation (Fig. 5d). In view of the similarity of natural *c*-axis fabrics, possibly developed in a flow regime intermediate between pure and simple shear, and the theoretically predicted fabrics expected for strictly pure and simple shear histories, it is suggested that the above notion by Platt & Behrmann (1986) for the case of intermediate non-coaxial flow regimes be followed, and the working hypothesis be adopted,that the central girdle segment of the fabric tends to orient itself orthogonal to the extensional flow apophysis.

As emphasized above, s_r values determined on the basis of Ghosh & Ramberg's (1976) analysis bear the implicit assumption of time–constant flow behaviour. Before considering alternative histories, it may be worthwhile to elucidate the kinematic framework for such a flow.

By its definition, s_r quantifies the degree of non-coaxiality, and hence the vorticity of the flow. According to Passchier (1987b), s_r is related to Truesdell's (1954) kinematic vorticity number w_k by:

$$s_r = \frac{\sqrt{1 - w_k^2}}{2w_k}.$$

The value of $s_r = 0.65$ obtained above corresponds to a kinematic vorticity number $w_k = 0.61$, and this value has been used to sketch the kinematic framework in respect to the flow apophyses in Fig. 11(b). Note again that the extensional flow apophysis (the x direction in Ghosh & Ramberg's analysis) has been taken parallel to the foliation, which results in a tentative orientation of the incremental stretching axes with respect to the fabric as shown in Fig. 12(b).

Finite strain

The optimal $R - \alpha$ curve shown in Fig. 9, and obtained under the assumption of a time–constant

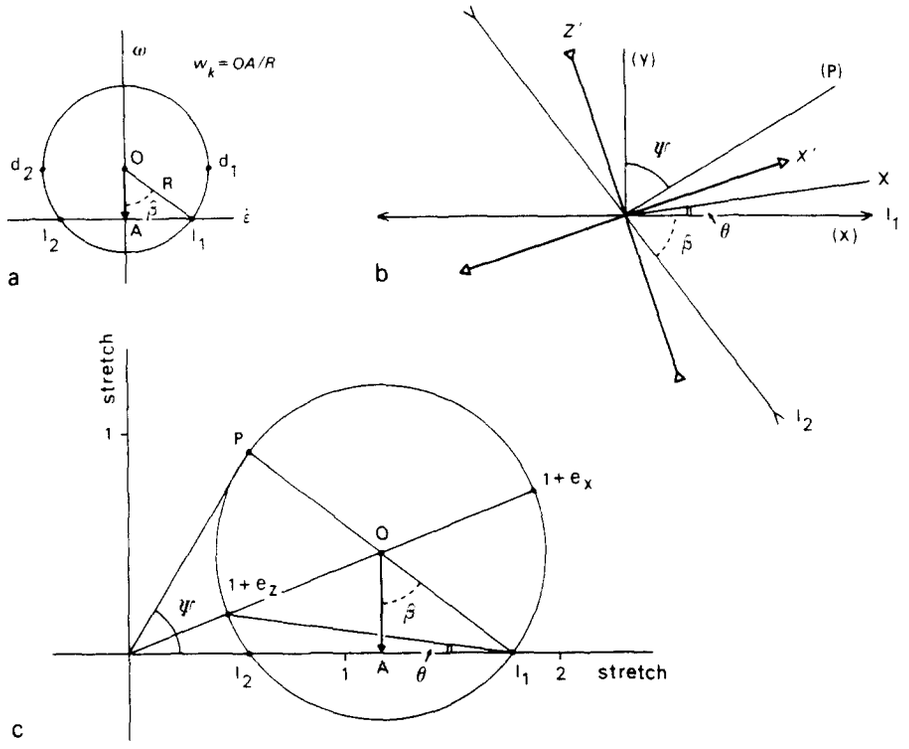

Fig. 11. (a) Mohr circle representation in $\dot{\varepsilon} - \omega$ space of non-coaxial flow. Intersections I_1 and I_2 represent flow apophyses. Kinematic vorticity number W_k = OA/R, with R the radius of the circle. (b) Kinematic framework for time–constant flow with $W_k = 0.61$, which would produce the $R - \alpha$ curve shown in Fig. 9. X' and Z' are the incremental extension and shortening directions, I_1 and I_2 the extensional and shortening apophyses of the flow. P denotes the end orientation of a line initially perpendicular to I_1, with ψ the angular shear. Co-ordinate axes x and y of Ghosh & Ramberg's analysis (Fig. 7) are shown bracketed. X is the finite extension direction calculated on the basis of the Mohr circle construction in (c), and oriented at an angle θ to the extensional flow apophysis. (c) Mohr circle representation in stretch space of the position gradients tensor that would result from time–constant flow with $W_k = 0.61$ and a shear strain of 1.645, needed to obtain the $R - \alpha$ curve in Fig. 9. A finite strain results with $X = 2.0$ and $Z = 0.5$, approximately. For further discussion see text.

vortical component of the flow, corresponds with a shear strain of 1.645. Passchier (1988) has shown that a time–constant flow behaviour of the flow allows the position gradients tensor for the finite state of the deformation to be established, and he showed that a Mohr circle representation of this tensor (Means 1982) will reflect the kinematic vorticity number of the flow in an off-axis location of the centre of the circle, analogous to its representation in the Mohr circle for that flow. The value of s_r, converted into W_k, and the value of the shear strain needed to attain the observed garnet rotation angles are sufficient to determine the Mohr circle for the position gradients tensor that would result from a deformation history with constant values of the

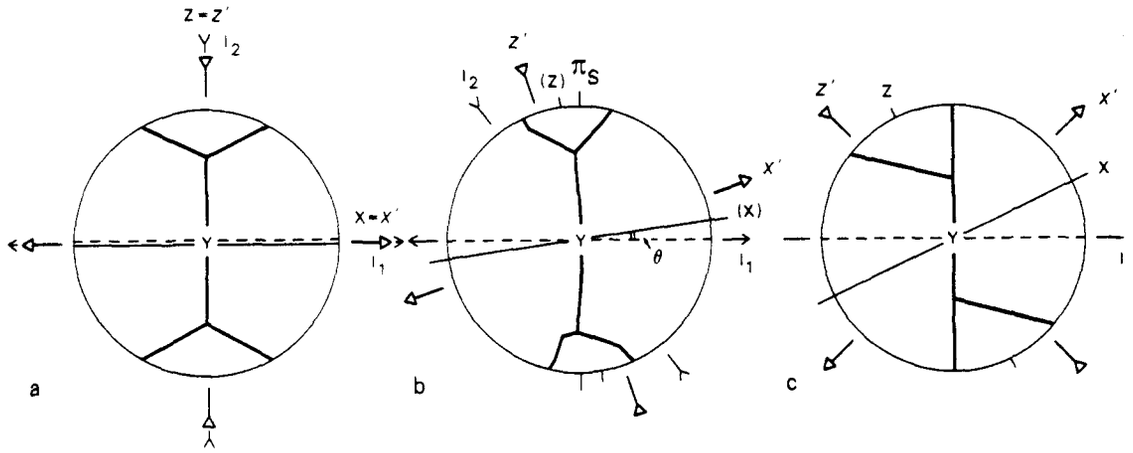

Fig. 12. Comparison of the fabric skeleton in specimen VV 194 with skeletal outlines predicted by Lister & Hobbs (1980) for progressive pure and simple shear. X' and Z' are the instantaneous stretching axes, X and Z the finite strain axes, I_1 and I_2 the extensional and shortening apophyses of the flow. (a) Fabric skeleton developed in model quartzite B (Lister & Hobbs 1980) under coaxial plane strain with $X = 2.0$. (b) Skeletal outline of c-axis fabric in specimen VV 194, with orientations of the kinematic framework shown in Fig. 11(b) and the finite strain ($X = 2.0$) in Fig. 11(c). π_s is pole to foliation. (c) Fabric skeleton developed in model quartzite B under progressive simple shear, at a shear strain of 1.5, X represents the finite extension direction ($X = 2.3$, approximately).

kinematic parameters. The resulting Mohr circle is shown in Fig. 11(c), and yields values for both the orientation θ and the magnitude of the finite strain, with $\theta = 8°$ and $1 + e_x = 2$, approximately (see also Fig. 12b).

Unfortunately, there are no independent strain markers to verify these numbers and the underlying assumptions, but it may be noted that the relatively low value of the strain obtained here could be one possible explanation for the lack of a distinct extension lineation, and further that the intensity of the fabric is consistent with that developed in simulated fabrics at comparable strain magnitudes (Lister & Hobbs 1980). However, such interpretations are necessarily tentative in view of the influence that migration recrystallization may have had on the development of the shape fabric as well as on the *c*-axis fabric intensity.

The deformation path

It has already been emphasized that the above analysis of the rotated garnets is inadequate to verify whether the flow was indeed constant with time in its kinematic description and that alternative two-stage histories may produce equal rotation angles for the observed range of aspect ratios. However, some constraints can be made on the basis of the simulation studies (Lister & Hobbs 1980) which emphasize that the fabric skeleton will rapidly track changes of the kinematic framework. A significant pure shear overprint (Fig. 10a) can thus be excluded, as such an overprint would result in a complete modification of the fabric skeleton into an internally symmetric type I crossed girdle. On the other hand, slight and possibly gradual changes of the flow regime during the waning stages are difficult to exclude, and a minor pure shear overprint, involving shortening close to the calculated finite Z axis (Fig. 12b) could certainly be consistent with the observed fabric pattern, not only with regard to the orientation of the peripheral legs but also with regard to the disposition of the pole-free areas (Fig. 5d). In this respect it is important to realize that the peripheral legs of a type I fabric are populated with *c*-axes corresponding to favoured orientations of the easily activated basal plane glide systems, whereas the central girdle segment is populated with *c*-axes of grains having the more difficult rhomb and prism systems in an adequate orientation for glide (Bouchez & Pêcher 1981, Schmid & Casey 1986, Mancktelow 1987). It may therefore be expected that changes of the kinematic framework during the closing stages of deformation at waning imposed strain rates will particularly affect the orientation of the peripheral legs: this renders a quantitative interpretation of the internal asymmetry of the fabric as defined by Behrmann & Platt (1982) extremely difficult.

One other notion has to be made here as to possible changes of the kinematic framework, to be expected even in the case of partitioning of the flow induced by a mechanical anisotropy. If this anisotropy initially made a large angle to the extensional apophysis of the bulk flow (or the flow plane in the case of bulk simple shear), a continuous and gradual repartitioning of the bulk vorticity between a shear-induced vorticity and rotation of the foliation (Lister & Williams 1983) would preclude a constant value of the shear-induced vorticity at the scale of the domain. In such cases vorticity numbers such as those obtained in this study will at best represent mean values built up during the local flow (Passchier 1988). It is suggested here that such numbers, calculated from the finite state of the deformation, be referred to as *finite vorticity numbers*, in order to emphasize that they only correspond to the kinematical vorticity number in the case of homogeneous flow with constant parameters. As the finite vorticity number determined from the garnet rotation angles necessarily reflects the cumulative effect of the entire deformation, whereas the skeletal outline of the fabric has been shown in the simulation studies to rapidly lose information on the earlier stages, it is quite possible that during the later stages of the deformation, reflected in the *c*-axis fabric, the kinematic vorticity number went through higher or lower values than the finite vorticity number.

Comparison with other fabrics

In view of the similarities of the *c*-axis fabric studied here with fabrics described by Behrmann & Platt (1982), Law *et al.* (1984), Platt & Behrmann (1986) and Schmid & Casey (1986) it may be interesting to compare the above results with possible values of the kinematic vorticity number associated with these other fabrics. From inspection of the Mohr circle in Fig. 11(c) it follows that the magnitude of the strain and the angle between the finite X axis and the extensional apophysis are sufficient to construct the Mohr circle for the position gradients tensor. On the basis of the strain data present in Platt & Behrmann (1986), and assuming that the central girdle segment of a type I fabric indeed orients itself orthogonal to the extensional flow apophysis, finite vorticity numbers of 0.94 and 0.59 follow for their mylonitic quartzites Pt 463 and B 102 in which the authors describe fabrics with a similar internal asymmetry. Such vorticity numbers give additional support to the idea that a spectrum exists of internally asymmetric fabrics related to flow regimes intermediate between pure and simple shear (cf. Schmid & Casey 1986).

CONCLUSIONS

(1) The *c*-axis fabric in the specimen is a type I crossed-girdle fabric with an asymmetric *c* axis distribution and an internally asymmetric fabric skeleton, developed under greenschist-facies conditions in a non-coaxial deformation history.

(2) The asymmetry of the *c*-axis distribution and the internal asymmetry of the fabric skeleton suggest a sense of vorticity, consistent with that inferred from extensional crenulation cleavages and asymmetric micro-boudinage, and consistent with the sense of rotation of the garnets.

(3) The quartz *c*-axes in the prekinematic garnet porphyroblasts show random patterns, indicating that the asymmetry of the *c*-axis distribution in the matrix results from the deformation history itself.

(4) The deformation history involved a pure shear component, either simultaneous with a component of simple shear at a constant ratio such that the kinematic framework remained constant with time, or at a ratio changing with time, for example as a late stage overprint.

(5) The microstructures indicating extension of the foliation, and the orthogonal orientation of the central girdle segment with respect to this foliation, suggest that flow at the scale of the specimen was controlled by the mechanical anisotropy due to the foliation. It is suggested that this anisotropy induced partitioning of the flow into shear parallel to the foliation, stretch of the foliation and rotation of the foliation. With the assumption of such partitioning, a finite vorticity number of 0.61 follows from the analysis of the rotated garnets, while the magnitude of the strain accumulated during garnet rotation and fabric development can be estimated at $1 + e_x = 2$.

(6) A number of uncertainties surround the deformation path and the orientation of the kinematic framework with time. Time–constant flow can explain the garnet rotation data, but a minor pure shear overprint is equally compatible with the garnet rotation data and the *c*-axis fabric, and this precludes a quantitative interpretation of the internal asymmetry. However, the orientation of the central segment of the fabric skeleton normal to the foliation indicates some direct relationship between the inferred flow regime and the observed fabric and, as a working hypothesis, it is suggested that this segment of the fabric skeleton tends to orient itself orthogonal to the extensional apophysis of the flow.

Acknowledgements—Gordon Lister, John Platt and Ide van der Molen are thanked for stimulating discussions during the earlier stages of this study. Many thanks are due to Cees Passchier for his interest, the invaluable discussions concerning flow analysis, and for giving the author access to his papers in preparation and in press. Detailed suggestions by Rick Law, Win Means and an anonymous reviewer have been of great help in shortening and improving of the text.

REFERENCES

Behrmann, J. H. & Platt, J. P. 1982. Sense of nappe emplacement from quartz c-axis fabrics; an example from the Betic Cordilleras (Spain). *Earth Planet. Sci. Lett.* **59**, 208–215.

Bouchez, J. L. & Pêcher, A. 1981. The Himalayan Main Central Thrust pile and its quartz-rich tectonites in central Nepal. *Tectonophysics* **78**, 23–50.

Carreras, J., Estrada, A. & White, S. H. 1977. The effects of folding on the c-axis fabrics of a quartz mylonite. *Tectonophysics* **39**, 3–24.

Diaz de Federico, A., Gomez-Pugnaire, M. T., Puga, E. & Torres-Roldan, R. 1978. Igneous and metamorphic processes in the geotectonic evolution of the Betic Cordilleras (southern Spain). *Cuad. Geol.* **8**, 37–60.

Egeler, C. G. & Simon, O. J. 1969. Sur la tectonique de la Zone betique (Cordilleres betiques, Espagne). *Verh. K. Ned. Akad. Wetensch. Afd. Natuurk.* **25**, 3, 1–90.

Eisbacher, G. H. 1970. Deformation mechanics of mylonite rocks and fractured granites in Cobequid Mountains, Nova Scotia, Canada. *Bull. geol. Soc. Am.* **81**, 2009–2020.

Etchecopar, A. 1974. Simulation par ordinateur de la deformation progressive d'un aggregat polycrystallin. Unpublished Ph.D. thesis, University of Nantes.

Etchecopar, A. 1977. A plane kinematic model of progressive deformation in a polycrystalline aggregate. *Tectonophysics* **39**, 121–139.

Garcia Celma, A. 1983. C-axis and shape fabrics in quartz mylonites of Cap de Creus (Spain): their properties and development. Unpublished Ph.D. thesis, State University of Utrecht.

Ghosh, S. K. & Ramberg, H. 1976. Reorientation of inclusions by combination of pure and simple shear. *Tectonophysics* **34**, 1–70.

Law, R. D., Knipe, R. J. & Dayan, H. 1984. Strain path partitioning within thrust sheets: microstructural and petrofabric evidence from the Moine thrust zone at Loch Eriboll, northwest Scotland. *J. Struct. Geol.* **6**, 477–497.

Leine, L. 1968. Rauhwackes in the Betic Cordilleras, Spain. Unpublished Ph.D. thesis, University of Amsterdam.

Lister, G. S. 1977. Discussion: Crossed girdle c-axis fabrics in quartzites plastically deformed by plane strain and progressive simple shear. *Tectonophysics* **39**, 51–54.

Lister, G. S. & Hobbs, B. E. 1980. The simulation of fabric development during plastic deformation and its application to quartzite: the influence of deformation history. *J. Struct. Geol.* **2**, 355–370.

Lister, G. S., Paterson, M. S. & Hobbs, B. E. 1978. The simulation of fabric development in plastic deformation and its application to quartzite: the model. *Tectonophysics* **45**, 107–158.

Lister, G. S. & Snoke, A. W. 1984. *S–C* mylonites. *J. Struct. Geol.* **6**, 617–638.

Lister, G. S. & Williams, P. F. 1979. Fabric development in shear zones: theoretical controls and observed phenomena. *J. Struct. Geol.* **1**, 283–297.

Lister, G. S. & Williams, P. F. The partitioning of deformation in flowing rock masses. *Tectonophysics* **92**, 1–33.

Mancktelow, N. S. 1987. Quartz textures from the Simplon Fault Zone, southwest Switzerland and north Italy. *Tectonophysics* **135**, 133–153.

Means, W. D. 1982. An unfamiliar Mohr circle construction for finite strain. *Tectonophysics* **89**, T1–T6.

Means, W. D. 1983. Application of the Mohr-circle construction to problems of inhomogeneous deformation. *J. Struct. Geol.* **5**, 279–286.

Passchier, C. W. 1983. The reliability of asymmetric *c*-axis fabrics of quartz to determine sense of vorticity. *Tectonophysics* **99**, T9–T18.

Passchier, C. W. 1986. Flow in natural shear zones—the consequences of spinning flow regimes. *Earth Planet. Sci. Lett.* **77**, 70–80.

Passchier, C. W. 1987a. Efficient use of the velocity gradients tensor in flow modelling. *Tectonophysics* **136**, 159–163.

Passchier, C. W. 1987b. Stable positions of rigid objects in non-coaxial flow—a study in vorticity analysis. *J. Struct. Geol.* **9**, 679–690.

Passchier, C. W. 1988. Analysis of deformation paths in shear zones. *Geol. Rdsch.* **77**, 309–318.

Platt, J. P. 1982. Emplacement of a fold-nappe, Betic orogen, southern Spain. *Geology* **10**, 97–102.

Platt, J. P. 1984. Secondary cleavages in ductile shear zones. *J. Struct. Geol.* **6**, 439–442.

Platt, J. P. & Behrmann, J. H. 1986. Structures and fabrics in a crustal-scale shear zone, Betic Cordillera, SE Spain. *J. Struct. Geol.* **8**, 15–33.

Platt, J. P., Behrmann, J. H., Martinez, J. M. & Vissers, R. L. M. 1984. A zone of mylonite and related ductile deformation beneath the Alpujarride nappe complex, Betic Cordilleras, S. Spain. *Geol. Rdsch.* **73**, 773–785.

Platt, J. P. & Vissers, R. L. M. 1980. Extensional structures in anisotropic rocks. *J. Struct. Geol.* **2**, 397–410.

Poirier, J. P. & Guillopé, M. 1979. Deformation induced recrystallization of minerals. *Bull. Mineral.* **102**, 67–74.

Powell D. & Treagus, J. E. 1970. Rotational fabrics in metamorphic minerals. *Mineralog. Mag.* **37**, 801–814.

Puga, E. 1971. Investigaciones petrologicas en Sierra Nevada occidental (Resumen Tesis de Doctorado). Unpublished thesis, University of Granada.

Ramberg, H. 1975. Particle paths, displacement and progressive strain applicable to rocks. *Tectonophysics* **28**, 1–37.

Ramsay, J. G. 1962. The geometry and mechanics of formation of "similar" type folds. *J. Geol.* **70**, 309–327.

Roermund, H. van, Lister, G. S. & Williams, P. F. 1979. Progressive development of quartz fabrics in a shear zone from Monte Mucrone, Sezia-Lanzo zone, Italian Alps. *J. Struct. Geol.* **1**, 43–52.

Roever, W. P. de & Nijhuis, H. J. 1963. Plurifacial alpine metamorphism in the eastern Betic Cordilleras (SE Spain) with special

reference to the genesis of the glaucophane. *Geol. Rdsch.* **53**, 324–336.
Rosenfeld, J. L. 1970. Rotated garnets in metamorphic rocks. *Spec. Paper geol. Soc. Am.* **129**, 1–105.
Schmid, S. M. & Casey, M. 1986. Complete fabric analysis of some commonly observed quartz *c*-axis patterns. In: *Mineral and Rock Deformation: Laboratory Studies—The Paterson Volume* (edited by Hobbs, B. E. & Heard, H. C.). *Am. Geophys. Un. Geophys. Monogr.* **36**, 263–286.
Schmidt, W. 1918. Bewegungsspuren in Porphyroblasten Kristalliner Schiefer. *S. B. Akad. Wiss. Wien, Abt.* 1 **127**, 293–310.
Schoneveld, C. 1979. The geometry and significance of inclusion patterns in syntectonic porphyroblasts. Unpublished Ph.D. thesis, State University of Leiden.
Simpson, C. 1980. Oblique girdle orientation patterns of quartz *c*-axes from a shear zone in the basement core of the Maggia nappe, Ticino, Switzerland. *J. Struct. Geol.* **2**, 243–247.
Simpson C. & Schmid, S. M. 1983. An evaluation of criteria to deduce the sense of movement in sheared rocks. *Bull. geol. Soc. Am.* **94**, 1281–1288.
Torres Roldan, R. L. 1979. The tectonic subdivision of the Betic Zone (Betic Cordilleras, Southern Spain): its significance and one possible geotectonic scenario for the westernmost alpine belt. *Am. J. Sci.* **279**, 19–51.
Truesdell, C. 1954. *The Kinematics of Vorticity*. Indiana University Press, Bloomington.
Vissers, R. L. M. 1977. Data on the tectonic and metamorphic evolution of the central Sierra de los Filabres, Betic Cordilleras, SE Spain. *Geol. Rdsch.* **66**, 81–90.
Vissers, R. L. M. 1981. A structural study of the central Sierra de los Filabres (Betic Zone, SE Spain), with emphasis on deformational processes and their relation to the Alpine metamorphism. *GUA Papers of Geology Ser.* 1, **15**, 1–154.
Vissers, R. L. M. 1987. The effect of foliation orientation on the inferred rotation axes and rotation angles of rotated porphyroblasts. *Tectonophysics* **139**, 275–283.
Westra, G. 1969. Petrogenesis of a composite metamorphic facies series in an intricate fault-zone in the SE Sierra Cabrera, SE Spain. Unpublished Ph.D. thesis, University of Amsterdam.
Zwart, H. J. 1962. On the determination of polymetamorphic mineral associations and its application to the Bosost area (Central Pyrenees). *Geol. Rdsch.* **53**, 38–65.

APPENDIX

The rate of rotation $\dot{\varphi}$ of an ellipsoidal inclusion with aspect ratio R in a viscous medium, deforming by the simultaneous combination of pure and simple shear is (Ghosh & Ramberg 1976, equation 4):

$$\dot{\varphi} = \dot{\gamma}(A \cos^2 \varphi + B \sin 2\varphi + C \sin^2 \varphi)$$

in which:

$$A = \frac{R^2}{R^2 + 1}, \quad B = \frac{s_r(R^2 - 1)}{R^2 + 1} \quad \text{and} \quad C = \frac{1}{R^2 + 1}$$

and where $\dot{\gamma}$ is the shear strain rate, φ the angle between the object long axis and the normal to the shear direction, and $s_r = \dot{e}_r/\dot{\gamma}$, hence the ratio of the rates of pure shear to simple shear, related to each other as sketched in Fig. 7.

The finite angle of rotation of the object ω_{obj} is obtained by integrating this rate of rotation equation between the limits of the initial orientation φ_o and the orientation φ at any other time, solving for φ, and subtracting the initial orientation φ_o. There are three types of solution (Ghosh & Ramberg 1976, equations 11–13) which follow for certain critical relations between the axial ratio R of the porphyroblast and s_r, and in each case the finite orientation of the object will depend on the axial ratio R, the value of s_r, the shear strain component γ, and the initial orientation φ_o, or:

$$\varphi = \varphi(R, s_r, \gamma, \varphi_o)$$

which implies that the finite angle of rotation ω_{obj} can in general form be written as:

$$\omega_{obj} = \varphi(R, s_r, \gamma, \varphi_o) - \varphi_o. \tag{A1}$$

The orientation φ_{mar} of a passive marker, initially oriented at an angle $90 - \varphi_{om}$ to the shear direction (Ghosh & Ramberg 1976, equation 16) is given by:

$$\varphi_{mar} = \arctan \left\{ \exp(2\gamma s_r) \tan \varphi_{om} + \frac{1}{2s_r} (\exp(2\gamma s_r) - 1) \right\}.$$

This yields a finite angle of rotation ω_{max} which depends on the value of s_r, the shear strain component γ, and the initial orientation of the marker φ_{om}, or:

$$\omega_{mar} = \varphi_{mar}(s_r, \gamma, \varphi_{om}) - \varphi_{om}. \tag{A2}$$

It follows that the finite rotation angle α of an ellipsoidal object with respect to a foliation considered to behave as a passive marker must be:

$$\alpha = \omega_{obj} - \omega_{mar}. \tag{A3}$$

The plane of the internal foliation in the garnets lies parallel to the long dimensional axes, which means that the initial orientations φ_o of the porphyroblasts were equal to the initial orientation φ_{om} of the foliation. This reduces equation (A3) to:

$$\alpha = \varphi(R, s_r, \gamma, \varphi_o) - \varphi_{mar}(s_r, \gamma, \varphi_o) \tag{A4}$$

and this equation has been used to calculate the $R - \alpha$ curves.